PCCP

Accepted Manuscript

ROYAL SOCIETY OF CHEMISTRY

www.rsc.org/pccp

Disentangling vibronic and solvent broadening effects in the absorption spectra of coumarin derivatives for dyes sensitized solar cells

Javier Cerezo[1,§], Francisco J. Avila Ferrer[1,2,§], Fabrizio Santoro[1,*]

March 6, 2015

1) CNR–Consiglio Nazionale delle Ricerche, Istituto di Chimica dei Composti Organo Metallici (ICCOM-CNR), UOS di Pisa, Area della Ricerca, via G. Moruzzi 1, I-56124 Pisa, Italy

2) University of Málaga, Physical Chemistry, Faculty of Science, Málaga, 29071, Spain

[§])these authors contributed equally to the work [*]) Author to whom correspondence should be addressed. email:fabrizio.santoro@iccom.cnr.it

Abstract

We simulate from first-principles the absorption spectra of five structure-related coumarin derivatives utilized in dye sensitized solar cells (DSSC), investigating the vibronic and solvent contributions to the position and width of the spectra in ethanol. Ground and excited state potential energy surfaces (PES) are modeled by

Density Functional Theory (DFT) and its time-dependent (TD) expression for excited state (TD-DFT). The solute vibronic structure associated to the spectrum is calculated by a TD formalism, accounting for both Duschinsky and temperature effects, while solvent inhomogeneous broadening is evaluated according to Marcus' theory, computing the solvent reorganization energy by the state-specific implementation of polarizable continuum model (PCM) within TD-DFT. We adopted both the standard hybrid PBE0 and the range separated CAM-B3LYP functionals showing that the latter performs better both concerning the vibronic and solvent-induced contributions to the absorption lineshape. The different predictions of the two functionals are then rationalized in terms of the charge transfer (CT) character of the transitions showing that, on this class of compounds, it is strongly dependent on the nuclear structure. Such a dependence introduces a bias in the PBE0 PES that have a drastic impact on the vibronic spectra. We show that both the intrinsic vibronic structure and the solvent broadening play a relevant role in differentiating the absorption width of the five dyes. In this sense, our results provide a guide to understand the sources of spectral broadening of this family of dyes, a valuable help for a rational design of new molecules to improve DSSC devices.

1 Introduction

Dye sensitized solar cells (DSSC)[1–5] emerged as an attractive low-cost alternative to silicon-based solar cells rapidly after they were first realized, more than two decades ago by O'Regan and Grätzel.[6] The properties of the dye play a crucial role in the light harvesting and in the injection of the photoexcited electron into the electric circuit and, in this respect, ruthenium based compounds have guaranteed remarkable performance. However, their relatively high cost and toxicity has prompted the investigation of DSSC based on organic dyes. Coumarins stand as a very interesting class of compounds, given

the fast injection rates observed to TiO_2 substrates,[7,8] and the availability of a large range of synthetic derivatives that exhibit markedly different properties.[9–12] Actually, by wisely selecting their molecular structure, the performance of coumarin-based DSSC has been significantly enhanced, by reducing aggregation problems and ameliorating both absorption and redox properties.

Computational tools have been extensively adopted to understand the spectroscopic and redox processes in DSSC, rationalize the experimental data and try to improve DSSC efficiencies,[13,14] providing some predictions of the performance of new coumarin dyes.[15] Since key properties to optimize the light harvesting are the intensity, the position and the width of the absorption spectrum of the selected dyes, the absorption process itself in DSSC has been extensively evaluated. However this has been mostly done by computing the excitation energies of candidate dyes[16–18] while only a few computational works have addressed the role of vibronic contributions.[19,20] Their inclusion is actually necessary to get a direct comparison with the experimental spectral lineshapes, since vibronic transitions affect both the spectral maximum and width and eventually determine the "color" of the dyes.[21,22]

In a system as complex as DSSC the absorption lineshape depends not only on vibronic effects, but also on the solvent, the adsorption on the semiconductor and possible dyes aggregations. Understanding the specific role of all these effects is mandatory to achieve an accurate spectroscopic simulation and, hopefully, it would help further improvements of DSSC performances.

As a step toward this goal, in this contribution we exploit modern computational techniques to disentangle the effect of solvent, temperature, and molecular vibrations on the absorption lineshape of a series of coumarin dyes in ethanol (EtOH). Concretely, we selected five structurally related coumarin dyes adopted in DSSC[9,10,23–25] which are reported in Figure 1 together with their power to current efficiency.[23,24]

In order to perform our study, we use a fully quantum model for the solute and a polarizable continuum for the solvent. Concretely, the vibronic structure due to the solute contribution to the spectrum is described at pure quantum level in harmonic approximation with time-independent (TI)[26–28] and time-dependent (TD)[29] approaches that allow to account for Duschinsky and temperature effects. Recently, Barone and coworkers highlighted the usefulness to integrate TI and TD calculations to investigate the vibronic absorption and emission spectra of different coumarin dyes.[30] The solvent contribution to the spectral width instead is accounted for by applying implicit solvent models where the inhomogeneous broadening is computed by the solvent reorganization energy,[29,31] according to the classical Marcus's theory.[32]

2 Computational Details

Electronic structure calculations for the solute were performed with the density functional theory (DFT) for the ground state (GS), and with its TD extension (TD-DFT) for the excited state (ES), adopting both the PBE0 hybrid functional (25% of HF exchange)[33,34] and the range separated hybrid functional CAM-B3LYP.[35] Ground-state and excited-state Hessians have been obtained respectively by analytical second-order differentiation of the energy and by numerical differentiation of the analytical TD-DFT energy gradients. For the time consuming characterization of the GS and (most of all) ES PES we adopted the convenient 6-31G(d) basis set. Such a choice has been shown to provide spectral lineshapes in nice agreement with the experiment for coumarin dyes[30] as well as for other several systems[27,36–39] The effect of the extension of the basis set to 6-311+G(d,p) on the vertical energies and charge transfer (CT) properties of the excited states of some of the investigated dyes has been evaluated. Solvent effects on equilibrium geometries and Hessians have been included by the Polarizable Contin-

uum Model (PCM),[40] using the standard Linear Response (LR) implementation (LR-PCM/TD-DFT),[41,42] for which analytical gradients are available,[43] in non-equilibrium regime (*neq*). The vertical transition energies at the LR-PCM optimized geometries are refined by means of State Specific (SS) PCM calculations (*neq* regime for ES and equilibrium (*eq*) regime for GS). Electronic calculations have been performed by using the Gaussian09 program.[44]

In order to characterize the CT properties of the GS→ES transition we performed the analysis proposed by Le Bahers, Adamo and Ciofini[45] with the CT program by Jacquemin.[46] Accordingly, the CT character is described in terms of the difference density from the initial to the final state, through the definition of three parameters: the amount of charge transfered Q_{CT}, computed as the integral of the positive part of the density, the displacement of the charge D_{CT}, obtained by the distance between the barycenters of the negative and positive regions, and the dispersion index (H_x, H_y, H_z) accounting for the spread of each region.[45] Large values of Q_{CT} and D_{CT} indicate a high CT character. Moreover, the overlap between the negative and positive density regions becomes smaller at the increase of D_{CT} with respect to H_ξ (being ξ the axis connecting the barycenters), so that for $D_{CT} > H_\xi$ a deficient description of the transition by standard hybrid functionals may be suspected.

Vibrationally resolved spectra have been computed in Franck-Condon (FC) approximation. The harmonic potential energy surfaces (PES) of the GS and ES states have been modeled by using Adiabatic Hessian (AH) approach,[47] that expands each PES around its own equilibrium structure and accounts for Duschinsky effect.[48] Model PES in solution are obtained at LR-PCM level; in order to include the SS-PCM corrections the computed spectra have been shifted along the energy axis by the amount E^{VT}(SS-PCM)-E^{VT}(LR-PCM), where E^{VT} is the vertical transition energy at the GS geometry. We used internal coordinates (bonds, angles and dihedrals obtained from the Z-

matrix) to describe the normal modes, since they are advantageous when facing large displacements between the initial and final state geometries.[49] For the most critical case, nkx-2753, comparison of AH spectra obtained in Cartesian and internal coordinates with those predicted by the Vertical Hessian (VH) model is reported in Figure S1 of Electronic supplementary information (ESI). Time-independent (TI) and time-dependent (TD) strategies were employed to compute the spectra at 0 K and 300 K, respectively. The TI method here employed is based on a partition of the possible transition in classes and a pre-screening technique and was described elsewhere.[27,26,28,50,51] Full-convergence spectra at room temperature were obtained by a TD approach based on an analytical expression of the finite-temperature time-correlation function;[52–57] implementation details can be found in ref 29. All the spectra calculations with either TI or TD strategies were performed by a development version of our code *FCclasses*.[58] TI calculations can also be performed with Gaussian 09[44] (see refs. 59,60). Beyond what is shown in ref. 29 the TD implementation is validated for the specific systems studied in this contribution in the ESI (see Figure S2), showing that it delivers exactly the same results as the TI method for c343 at 0 K.

According to the protocol described in ref. 31, the inhomogeneous broadening was simulated with a Gaussian lineshape whose standard deviation σ_m is estimated from the solvent reorganization energy λ using the Marcus' expression[32]

$$\left(\sigma_m\right)^2 = 2k_b T\lambda \tag{1}$$

The solvent reorganization energy (λ) was obtained as difference of *neq* and *eq* vertical transition energies (λ=$E^{VT}(neq)$- $E^{VT}(eq)$) computed with the SS implementation of PCM within TD-DFT (SS-PCM/TD-DFT).[41,61,62] In the framework of the PCM and

of other continuum solvation models, *neq* and *eq* time-regimes are simply ruled by two different dielectric constants. Equilibrium solvation is ruled only by the static dielectric constant. On the contrary, in the *neq* case, the reaction field due to the fast solvent degrees of freedom depends on the dielectric constant at optical frequency (ε_{opt}, usually related to the square of the solvent refractive index, $\varepsilon_{opt} = n^2$).

In this work, we primarily focus on the width of the spectra of the coumarin dyes in solution, mainly adopting two measures: the standard deviation defined as $\sigma = \sqrt{\mathscr{M}_2 - \mathscr{M}_1^2}$ (where $\mathscr{M}_1$ and $\mathscr{M}_2$ are respectively the first and second moments of the spectrum lineshape), and the full-width at half-maximum (FWHM, in the following indicated in short as W). The standard deviation is the most convenient measure for comparing computed spectra since it can be defined for both high-resolution and low-resolution spectra and its square (the variance) is additive for convoluted spectra (e.g. the variance of the total spectrum in polar solvents, σ_{tot}^2, is simply the sum of the vibrational σ_{vib}^2 and solvent σ_m^2 contributions). The FWHM is on the contrary useful for comparison with experimental spectra where σ can be seldom defined with precision due to truncation or overlap with the spectra due to other electronic states. For the Gaussian solvent contribution by definition $W_m = \sigma_m \sqrt{8ln2}$.

3 Results and Discussion

The five dyes sketched in Figure 1 share the same coumarin fused-ring core structure, while they differ in the length and substituents of the conjugated chain carrying the carboxylic function that anchors the dye on TiO_2 in DSSC. For all the dyes, the spectra arise from the $S_0 \rightarrow S_1$ transition, which corresponds to an excitation from the Highest Occupied Molecular Orbital (HOMO) to the Lowest Unoccupied Molecular Orbital (LUMO); plots of HOMO and LUMO for each molecule are given in Section S2 in the

ESI.

The dyes under investigation are complex systems and can exist in several different forms. They are weak acids so that an equilibrium takes place between the neutral (protonated) and anion species. The pKa of c343 in water is 6,[63] and it increases in less polar solvents (is 7.3 in a 4:1 dioxane-water mixture[64]). Since we are interested in the spectra in EtOH only the neutral species are considered. Different protomers are possible and those selected are sketched in Figure 1. Detailed tests were performed for c343, for which we considered two protonation isomers (Figure 1): c343-I, characterized by the intramolecular hydrogen bond O_1-H_1...O_2 and c343-II where the dihedral $H_1O_1C_1C_2$ is 180 degrees. We found that the c343-I is more stable than II by 6 kcal/mol (see Figure S3 in the ESI), so that it should be the most populated at room temperature, in agreement with what found by Wu and co.[19] It is worthy to add that, in any case, according to our simulations the two protomers have very similar absorption spectra, and the vertical energy for (I) is predicted to be only 0.03 eV lower than for (II) in EtOH. Other possible protomers are less stable[65] and were not considered.

Finally, the investigated dyes exist at room temperature in few different conformations depending on the *syn* or *anti* arrangements around the Nitrogen atom. The different conformers exhibit very similar absorption spectra and, in the following, we only consider *anti* species.

In order to disentangle the role of the structural and solvent effects we simulate the spectra of the five dyes both in gas-phase and ethanol (EtOH) solution. For c343 we also considered polar aprotic solutions.

3.1 Charge Transfer Character of the Electronic Transitions

The proper description of S_1 excited states of coumarins requires an adequate treatment of its CT character.[18] In this sense, standard hybrid functionals, namely B3LYP, have

revealed some limitations, leading to a significant underestimation of the vertical energy as the size of the dye increases,[17] while range-corrected functionals provide a much better description.[18] Nevertheless, based on the performance of hybrid PBE0 functional,[15] up to now the CT effect was judged only moderate for medium sized coumarins as those investigated in this paper.

The vertical transition energies, E^{VT}, computed with both PBE0 and CAM-B3LYP functionals according to LR-PCM and SS-PCM implementations are reported in Table 1. SS-PCM values in EtOH are generally red-shifted with respect to LR-PCM ones and the shift tends to be larger for the species undergoing the larger polarity change during the optical transition (see Table 2) namely nkx-2586 and nkx-2753; however some exception exists (see nkx-2311). As expected from previous works[18] the relative energies of the different dyes are better reproduced by CAM-B3LYP than by PBE0. In fact, while the energy gap between the most blue (c343, 2.78 eV) and the most red (nkx-2586, 2.43 eV) experimental absorption maxima is 0.35 eV, it is 0.76 (LR-PCM) and 0.78 (SS-PCM) eV according to CAM-B3LYP and it increases to 0.94 eV according to PBE0 (both LR and SS results). On the contrary, considering absolute energies, CAM-B3LYP introduces larger blueshift with respect to experiment than PBE0 for the smaller species.

A more in depth comparison with experiment requires the simulation of the whole lineshape of the absorption spectrum.[66] This is done in the next sections computing the spectra according to SS-PCM vertical energies, better suited than LR-PCM to predict solvatochromic effects for transitions with remarkable CT character and to compute solvent reorganization energies.[29,31]

Here, as a preliminary step, we analyzed the CT character of the $S_0 \rightarrow S_1$ transition of the five coumarin dyes by means of the parameters suggested by Le Bahers et al.[45] Such CT parameters have been computed for every molecule in its GS and ES minima using

either PBE0 or CAM-B3LYP functional. Table 2 shows that, independently of the functional, the CT character is significant both considering the Q_{CT} and D_{CT} parameters, and it increases with the size of the dye, i.e., it is higher for the dyes with longer conjugated chain (nkx-2586 ad nkx-2753) and, consequently, the change of electric dipole moment is also larger. The positions of the barycenters of positive and negative charges are reported in Figure S4 in the ESI. The significant CT character observed for the large coumarins, along with the well known limitations of standard hybrids to describe charge transfer (CT) states[67] (notice that $D_{CT} > H_x$) , provides a rationale to understand the differences obtained with CAM-B3LYP and PBE0.

Table 2 shows that according to CAM-B3LYP the CT character decreases significantly from the FC geometry to the ES minimum for all the dyes. A similar trend is seen in PBE0 results (apart for c343) but differences are smaller. For the larger members of the series such dependence on the coordinates of the CT character modulates the relative accuracy of PBE0 along the ES PES, and this introduces a bias that affects the position of the minimum on the ES PES (see section S4 in the ESI for further details). As a consequence, with respect to CAM-B3LYP predictions, at PBE0 level the bond order alternation from GS to ES is remarkably smaller. This leads to reduced vibrational progressions along the C=C stretching modes of the polyenic chain and to vibronic spectra very similar for all the five dyes (see below and Figures S5-S8 in the ESI). On the contrary, as shown in the next section, CAM-B3YP progressions are stronger for the larger dyes and this parallels the increase of the spectral width observed in experiment.

3.2 Vibrational Structure of the spectra

We start this analysis assigning the normal modes responsible for the different bands observed in the high resolution spectra. To that end we focus on the smallest species c343 and one of the largest ones, nkx-2753, and we plot in Figure 2 the stick spectra

computed with the TI approach at 0 K. Animations of the most relevant CAM-B3LYP normal modes are given as ESI. According to CAM-B3LYP results, nkx-2753 is the dye with the largest vibronic structure and the three major bands of the convoluted line shape arise from a progression along a C=C(st) ('st' stands for stretching) mode of the polyenic side chain. The lowest-energy band mainly comprises a progression along in-plane bendings of the molecule as a whole where the individual rings are displaced almost rigidly ("Molec. bending"). On the contrary, the shoulder at $\sim$ 600-700 cm^{-1} above the 0-0 transition is related to a collective motion of the internal bendings of the coumarin rings ("Coum. ring (bend)"). The spectra of the other coumarins exhibit similar features but with different relative intensities (see TD spectra at 0 K in Figure 3). The dye most closely related dye to nkx-2753 is nkx-2586 (stick spectrum not shown), since it only differs for the lack of the alkyl ring within the polyenic chain; the differences perceivable in the spectra of these two species at 0 K arise from the contribution of additional transitions related with the torsion of this ring. Indeed, the perturbation of the ring structure upon bond length alternation, induces a displacement of such modes, resulting in the larger vibronic broadening and temperature effects for nkx-2753. According to CAM-B3LYP predictions, as the size of the side chain decreases, the C=C(st) progressions are reduced; this observation can be put on a quantitative base by looking at the dimensionless displacements associated with the most FC active C=C(st) mode for each dye, which are 1.18 (nkx-2753), 1.32 (nkx-2586), 0.85 (nkx-2311), 0.60 (nkx-2398) and 0.30 (c343). Furthermore, for the larger dyes, the progression along the mode indicated as "Molec. bending" is enhanced, because it gains a contribution from the polyenic chain; in turn, as shown in Figure 3 the resolution of the low-energy band at 300 K decreases and in fact the width at half-height of such band cannot be defined for nkx-2753 and nkx-2586 since it coalesces into the adjacent peak.

The above analysis highlights the leading role of C=C(st) progressions in the vi-

bronic spectra, further explaining why the dyes with larger conjugated chains are those with a larger vibronic width, in good agreement with the experimental trends. It is interesting to notice that although the carbonyl, carboxylic and nitrile groups have a clear impact on the electronic transitions of the different dyes, the vibrations of these functional groups do not contribute with remarkable progressions to the spectra, except in the case of c343, for which the C=O(st) associated with the carbonyl of the coumarin ring shows a intensity similar to that of C=C(st).

The main stick bands computed with PBE0 are assigned to similar normal modes, but their intensities are remarkably different from those predicted by CAM-B3LYP. The C=C(st) progressions of the larger molecules are drastically reduced, indicating a much lower bond alternation from S_0 to S_1. As a result, the differences between the vibronic progressions of the different dyes are much smaller and, even, the trend is opposite. In fact, as shown in Figure 2(b,d), the spectrum appears broader for c343 than for nkx-2753. As discussed above, the different predictions of the two functionals can be traced back to an inaccurate evaluation of the ES PES with PBE0 due to the CT character of the state. Analogous problems were recently observed on the vibrational reorganization energy of CT states by Silverstein et al.[68]

Figure 3 reports the vibrationally resolved spectra of the five dyes at 0 K, computed at CAM-B3LYP/6-31G(d) level of theory in ethanol and convoluted with a narrow Gaussian lineshape (FWHM=180 cm^{-1}) and confirms the generality of the trend observed in Figure 2 for CAM-B3LYP predictions: the larger is the coumarin the broader is the vibronic spectrum. Moreover a net red-shift is observed at the increase of the size of the dye, in agreement with the E^{VT} data in Table 1.

Increasing the temperature from 0 to 300 K, progressions along low-frequency normal modes lead to a broadening of the spectra. More in detail, for all the dyes but nkx-2753, Figure 3 shows a moderate temperature effect that broads every single band

without altering the relative intensity of the main vibronic features. For nkx-2753, the effect of the temperature is more significant and remarkably changes both the width and the shape of the spectrum. According to our band assignment, this differentiated behavior is a consequence of the displacement of the low frequency modes associated with the additional alkyl ring of this dye.

The above analysis is confirmed by the standard deviations of the vibronic spectra σ_{vib} (Table 3). For all dyes except nkx-2753, the increment from 0 K to 300 K is $\sim 5\%$, while in the case of nkx-2753 it reaches 10%. As we will show in the next section, such a thermal broadening leads to a total width of the computed spectrum of nkx-2753 that is larger than what observed experimentally. For this dye, section S1 in the ESI shows that AH predictions with internal coordinates (used here) are very similar to vertical Hessian (VH)[47] results and narrower than AH results adopting Cartesian coordinates, and this supports the reliability of our calculations. However, to further assess the reliability of the predicted broadening it would be necessary to include anharmonic effects along the low-frequencies modes of the alkyl ring.

Figure 3 reports also the PBE0/6-31G(d) spectra at 300 K showing that they predict much more similar lineshapes for the different dyes with respect to CAM-B3LYP results. This finding is in line with what noticed in the high resolution spectra of c343 and nkx-2753 in Figure 2.

3.3 Solvent effects on the absorption spectra

Maxima and widths of the experimental spectra of the investigated dyes in EtOH are collected in Tables 3, 4, and 5 and show an interesting correlation between the solvatochromism and the widths of the spectra: the more red-shifted is the spectrum (Table 4), the broader is its lineshape (Table 5). The experimental spectra in EtOH (Figure 4(b)) of the larger systems (nkx-2311, nkx-2586 and nkx-2753) are remarkably broader

than those of the smaller systems (c343 and nkx-2398). In the previous section we have shown that, according to CAM-B3LYP results, the vibronic contribution to the spectral width changes remarkably for the different systems and follows the experimental trend, while this is not true for PBE0 predictions (see Figure 3).

We now turn to investigate the solvent effect on the vibronic structures and on the spectral widths.

3.3.1 Solvent effect on the vibronic lineshape

We start discussing the solvent effect on the GS and ES equilibrium geometries and normal modes. To that end in Figure 3 we compare spectra in ethanol and in gas phase (GP) at 300 K. As expected, the GP spectra are blue-shifted with respect to those in EtOH, with a shift of $\sim$ 0.4-0.5 eV. Let us now focus on the lineshapes. On the balance the relative position and intensities of the vibronic peaks in ethanol and in gas-phase are rather similar. Going into further details, Figure 3 indicates that the differences between the spectra in GP and EtOH depend on the actual dye. For the smaller systems (c343 and nkx-2398), the spectra in GP are broader than the EtOH ones, following the same trend already observed for other systems like coumarins C153.[29,69] However, as the size of the dye increases, the effect is gradually inverted: the medium sized nkx-2311 shows similar widths in GP and EtOH, and the larger dyes, nkx-2586 and nkx-2753, display the opposite behavior, as the EtOH spectra are broader than the GP ones. Such differences indicate a larger geometric change between the GS and ES minima in EtOH for the larger dyes. According to the assignments provided in Section 3.2, the vibrational progressions for the larger dyes are mainly contributed by the C=C(st) modes and, consequently, the larger progression in EtOH can be traced back to a larger bond order alternation in the polar solvent. In Figure S5 in the ESI we show that analogous differences between GP and EtOH spectra are already observed at 0 K. Furthermore, in Figures S7

and S8, we also compare PBE0 results in GP and EtOH at 0 K and 300 K, showing that they display a similar behavior, although the differences between GP and EtOH spectra for the larger dyes are even smaller than those obtained with CAM-B3LYP.

3.3.2 Broadening effect according to continuum models

According to Marcus' theory the broadening due to the polar interactions of the solvent can be traced back to a single descriptor: the solvent reorganization energy (λ). The values computed at SS-PCM/TD-CAM-B3LYP level both at the GS and ES minima are reported in Table 7. According to the FC principle, in order to estimate the broadening in absorption we considered the λ values taken at the S_0 minimum. These latter follow a clear trend, increasing at the increase of the size and the CT character of the $S_0 \rightarrow S_1$, as expected from the fact that the electrostatic interactions between the polar solvent and the solute are enhanced.

Figure 4 compares the experimental spectra (b) with the final computed spectra obtained by convoluting the CAM-B3LYP (a) and PBE0 (c) vibronic lineshapes with the solvent Gaussian broadening (the σ_m values are given in Table 3). As observed in this figure, CAM-B3LYP simulations provide a set of spectra with lineshapes in nice agreement with the experimental ones, while PBE0 simulations are significantly narrower. This is confirmed from the analysis of the FWHMs of the simulated and experimental spectra, shown in Table 5. To allow a more direct comparison, Figure 5 reports the spectra in EtOH of all coumarins except c343 (which is shown in Figure 6) computed with CAM-B3LYP and PBE0 and shifted according to the energy of their spectral maxima. The better performance of CAM-B3LYP with respect to PBE0 is evident. More in detail, the agreement of CAM-B3LYP spectra with experiment is excellent for dyes nkx-2398 and nkx-2586, while the spectral width of nkx-2753 is slightly overestimated and that of nkx-2311 and c343 are underestimated. The slight mismatch for nkx-2753

probably arises from the overestimation of the vibrational contribution at room temperature, discussed in the previous section, and therefore it may be due to an inaccurate treatment of the large-amplitude anharmonic distortions of the alkyl ring. The reasons for the underestimation of the width of nkx-2311 and c343 spectra are likely different: the experimental spectrum of nkx-2311 is more symmetric than the computed one and this would suggest that the estimated inhomogeneous broadening is too small for this molecule. In order to test this hypothesis it would be helpful to compare with an experimental spectrum in a low-polarity solvent, but we were not able to find it in literature. At variance, for c343 the experimental band still shows a remarkable asymmetry, indicating that, most probably, in this case the vibrational structure is being underestimated.

To investigate further this hypothesis we simulated c343 spectra in polar aprotic solvents, as 1,2-dichloroethane (DCE) and acetonitrile (ACN, more polar than EtOH); they are reported in Figure 6. In these cases the simulated spectra compare pretty well with the experiment[9,25,70] (see also Table 6), and the slight differences can be related with the fact that non-electrostatic contributions are not considered in our estimate of the solvent broadening based on PCM calculations.[31] Therefore, it is reasonable to assume that the remarkable differences seen in EtOH are due to a change in the vibronic structure due to solute/solvent hydrogen bonds. In order to check this, it would be necessary to adopt cluster models and include explicit solvent molecules in the vibronic calculations. C343 and the other coumarin dyes here investigated can also give rise to aggregates, which may have an impact on the absorption spectra due to the coupling between the excitons and the vibrations. In fact, this latter potentially causes a redistribution of the vibronic intensities, and the appearance of new lines originating both from intramolecular and intermolecular vibrations that can determine a broadening of the spectra. However aggregates formation is more likely in nonpolar solvents.[63,65]

A detailed investigation of all these possible effects lie outside the scope of the

present work, which is focused on the performance of simple implicit models to simulate the effect of the solvent in the spectroscopic bands of the whole series of selected coumarins. In this respect, we showed that on the balance, when coupled with a suitable functional, the model adopted for the solvent inhomogenoeus broadening performs nicely in the investigated cases, reproducing the experimental trend and delivering total spectra in satisfactory agreement with experiment. Nonetheless, it is important to close this section with a caveat. At variance with what we observed for coumarin C153,[29,31] for the investigated series of dyes the reorganization energies change remarkably along the ES PES, from the FC region to the minimum (Table 7). Focusing on CAM-B3LYP estimations, the reorganization energies drop at the ES minimum compared with those at the FC region, and they reach similar values for all the nkx-family dyes. This behavior can be explained noticing that, as reported in Table 2, the CT character is reduced from the FC point to the ES minimum and, consequently, the same happens to the change of the dipole moment from GS to ES (also included in Table 2), thus leading to lower reorganization energies. These data indicate that for the examine coumarin dyes the solvent reorganization is inherently coupled to the geometric relaxation of the solute. This effect cannot be taken into account in the simple model we adopted to address the solvent broadening. In fact, being based on a convolution of the vibrational and solvent lineshapes, it implicitly assumes that solvent and solute degrees of freedom are negligibly coupled. Future work will be devoted to a careful analysis of the potential effects arising from such couplings.

3.4 Relative performance of PBE0 and CAM-B3LYP

The simulation of the vibronic spectra provides a very suitable framework to assess the ability of both PBE0 and CAM-B3LYP functionals to characterize the spectroscopic features of the selected family of coumarins. In the previous section it was clearly

shown that CAM-B3LYP outperforms PBE0 as far as the simulation of the lineshapes is concerned.

Let us consider the predictions on the band positions. The availability of the whole lineshape, as opposed to calculation of the vertical energies, allows a direct comparison with the experimental spectral maxima (Table 4). It was already highlighted that vibronic effects can cause systematic differences between the spectral maxima and the vertical transition energies,[71] and this is what happens in our systems. The comparison of the simulated spectral maxima, ω^{max} (Table 4), and the vertical energies, E_V (Table 1), indicates that the two parameters are displaced by an amount that is different for each system, as a consequence of the different vibrational structure. Concretely, the computed ω^{max} and E^{VT} differ by 0.24 eV for the asymmetric spectrum of c343 while they come closer as the broadening of the spectrum increases, nearly matching one each other for nkx-2753. This has an impact on the estimate of the error, actually leading to a better comparison with experiment. In fact, let us consider once more, as done in Section 3.1, the energy gap between the experimental maxima of c343 and nkx-2586 dyes (0.35 eV). We showed that considering the E^{VT} difference the error of SS-PCM/CAM-B3LYP/6-31G(d) data is 0.43 eV. Introducing vibronic and solvent effects the error is actually reduced to 0.38 eV. The error instead is 0.5 eV according to PBE0. Additionally, this functional incorrectly predicts that the nkx-2753 spectrum is red-shifted with respect to the nkx-2586 one.

The ω^{max} computed with CAM-B3LYP are systematically blueshifted with respect to the experimental values, with differences of ~ 0.4 eV for c343, ~ 0.35 eV for nkx-2398 and ≤ 0.15 eV for nkx-2311, nkx-2586 and nkx-2753. On the contrary, the differences between the experimental ω^{max} and the simulated values with PBE0 show a larger dispersion, as they range from slightly blueshifted bands (c343 and nkx-2398) to remarkably redshifted ones (nkx-2586 by ~ 0.3 eV and nkx-2753 by ~ 0.4 eV), with a

nice match for nkx-2311 (0.08 eV). This result is consistent with the flaws of PBE0 in dealing with CT states. On the balance, the relative position of the dyes is better reproduced with CAM-B3LYP, and this is an important feature in order to reliably predict the effect of new substituents in the development of improved dyes for DSSCs. it should be noted that a further improvement of CAM-B3LYP predictions would be possible increasing the basis set. In fact, E^{VT} for c343 and nkx-2586- decreases by respectively 0.14 and 0.09 eV by extending the basis set from 6-31G(d) to 6-311+G(d,p). Interestingly, both the solvent reorganization energy and the CT character remain mostly unaffected by the change of the basis set.

4 Summary and Conclusions

In this work we investigated the absorption spectra in ethanol of a family of five coumarin derivatives structurally related and adopted in dye sensitized solar cells. Light harvesting is a crucial step in the DSSC operation and in fact the efficiency of these dyes tend to increase with the width of the absorption spectra and the shift of the maxima toward the red (although, probably due to aggregation issues,[24] nkx-2586 seems to deviate from this trend, as it can be seen from the data in Figure 1 and Tables 4 and 5). On these grounds, in the present work we aimed at understanding what determines the shape of the absorption spectra of these dyes in ethanol, dissecting the role of vibronic and solvent contributions. To that end we profited of the recent possibility to efficiently compute vibronic spectra also including temperature effects,[29] and we exploited recent strategies to estimate the solvent inhomogeneous broadening from continuum solvent models.[31]

In summary, we have shown that both vibronic and solvent broadening effects are important and they concur to increase the spectral width as the length of the conjugated

side chain attached to the coumarin core become longer. Both contributions are connected with the increase of the CT character of the electronic transition. This connection also explains why CAM-B3LYP provides results in better agreement with experiment than PBE0. Indeed, the limitations of PBE0 to accurately treat CT states, makes CAM-B3LYP a much more reliable theoretical method to investigate the photophysics of these molecules. It is interesting to notice that, although comparison of Figures 4 and 3 evidences a spectacular effect of the inhomogeneous broadening on the computed lineshape, the dominant contribution to the spectral width is, in any case, represented by the vibronic structure as it clearly seen from the standard deviations reported in Table 3.

Concerning the vibronic contribution, we have shown that the increase with the length of the conjugated chain is due to the enhancement of the progressions arising from the related C=C stretching modes. Nonetheless also low-frequency modes play a role and in fact thermal broadening induces a mild, yet noticeable, increment of the vibrational width and contributes markedly to the loss of the vibrational resolution.

Solvent effects on the vibronic structure are moderate. On the contrary, the EtOH environment gives a remarkable contribution to the spectral width accentuating the differences among the dyes already present at vibronic level. The solvent broadening is nicely captured by application of Marcus' theory on the grounds of solvent reorganization energies computed with SS-PCM. Such broadening is predicted to be larger for those dyes whose excited states show a larger CT character, i.e., in the order c343$<$nkx-2398$<$nkx-2311$<$nkx-2586$\sim$nkx-2753. On this respect, however it should be noticed that the CT character of the excited state, and consequently the solvent reorganization energy, is significantly reduced moving from the GS to the ES minimum. Such a dependence of the solvent response on the solute nuclear coordinates is not considered in our model (see Section 3.3.2) and calls for future studies.

In general, the final predicted spectra in EtOH computed with CAM-B3LYP, are in

good agreement with experiment both in absolute terms (position and width) and even more as far as their relative differences are concerned. Therefore these calculations suggest that the H-bonds with the solvent not described by PCM do not significantly contribute to the spectral broadening. In this respect, however, c343 shows some specificity, since a simple Gaussian convolution added to the vibrational structure is not able to provide an accurate reproduction of the strongly asymmetric lineshape in EtOH, contrarily to the results obtained in polar aprotic solvents, such as DCE or ACN. It is possible that for c343 in protic solvents the vibrational structure is significantly perturbed by specific solute-solvent interactions, e.g. through formation of hydrogen bonds. The contribution of such vibrations to the width of the vibronic structures has been recently documented for N-methyl-6-oxyquinolinium betaine in water.[69] It is plausible that, in the investigated series of coumarins, this effect may be more visible for the dyes showing the narrower spectra as c343, although the role of possible protomers equilibria should also be considered. Further work to explore these possibilities for the systems analyzed in this work is currently in progress on the grounds of explicit solvation models and it will be reported in a forthcoming contribution. Future work will also be devoted to the study of the effect on the absorption spectra due to the chemisorption on the semiconductor surface.

Acknowledgments The authors acknowledge the support of the Italian Institute of Technology (IIT-Seed HELYOS) and MIUR (PRIN Project no. 2010ERFKXL_008). FA acknowledges support from the Marie Curie COFUND programme U-Mobility, co-financed by the University of Malaga, the European Commission FP7 under GA No. 246550, and Ministerio de Economía y Competitividad (COFUND2013- 40259). JC thanks "Fundación Ramón Areces" (Madrid, Spain) for funding his postdoctoral position, and the Pisa Unit of ICCOM-CNR Pisa for hospitality. The authors acknowledge several useful discussions with dr. Giacomo Prampolini (CNR–ICCOM, Pisa).

Electronic supplementary information (ESI) available. Comparison of VH spectra and AH spectra computed either in Cartesian or in internal coordinates and comparison of TD and TI spectra for C343 at 0 K; plots of the HOMO and LUMO for the different chromophores; relative stability of the protomers of C343; further analysis on the CT character and its effect on FC factors; for nkx-2753 further comparisons of CAM-B3LYP and PBE0 spectra in gas-phase and in ethanol. Animations of the most relevant modes of c343 and nkx-2753 at CAM-B3LYP level.

References

[1] M. Grätzel, *Pure Appl. Chem.*, 2001, **73**, 459–467.

[2] S. Ardo and G. J. Meyer, *Chem. Soc. Rev.*, 2009, **38**, 115–164.

[3] J.-L. Brédas, J. E. Norton, J. Cornil and V. Coropceanu, *Acc. Chem. Res.*, 2009, **42**, 1691–1699.

[4] O. V. Prezhdo, W. R. Duncan and V. V. Prezhdo, *Acc. Chem. Res.*, 2008, **41**, 339–348.

[5] A. Hagfeldt, G. Boschloo, L. Sun, L. Kloo and H. Pettersson, *Chem. Rev.*, 2010, **110**, 6595–6663.

[6] B. O'Regan and M. Grätzel, *Nature*, 1991, **353**, 737–740.

[7] M. K. Nazeeruddin, A. Kay, I. Rodicio, R. Humphry-Baker, E. Mueller, P. Liska, N. Vlachopoulos and M. Graetzel, *J. Am. Chem. Soc.*, 1993, **115**, 6382–6390.

[8] M. K. Nazeeruddin, P. Pechy and M. Gratzel, *Chem. Commun.*, 1997, 1705–1706.

[9] K. Hara, K. Sayama, Y. Ohga, A. Shinpo, S. Suga and H. Arakawa, *Chem. Commun.*, 2001, 569–570.

[10] K. Hara, T. Sato, R. Katoh, A. Furube, Y. Ohga, A. Shinpo, S. Suga, K. Sayama, H. Sugihara and H. Arakawa, *J. Phys. Chem. B*, 2003, **107**, 597–606.

[11] K. Hara, M. Kurashige, Y. Dan-oh, C. Kasada, A. Shinpo, S. Suga, K. Sayama and H. Arakawa, *New J. Chem.*, 2003, **27**, 783–785.

[12] K. Hara, Z.-S. Wang, T. Sato, A. Furube, R. Katoh, H. Sugihara, Y. Dan-oh, C. Kasada, A. Shinpo and S. Suga, *J. Phys. Chem. B*, 2005, **109**, 15476–15482.

[13] F. Labat, T. Le Bahers, I. Ciofini and C. Adamo, *Acc. Chem. Res.*, 2012, **45**, 1268–1277.

[14] T. Le Bahers, T. Pauporté, P. P. Lainé, F. Labat, C. Adamo and I. Ciofini, *J. Phys. Chem. Lett.*, 2013, **4**, 1044–1050.

[15] R. Sanchez-de-Armas, M. A. San Miguel, J. Oviedo and J. F. Sanz, *Phys. Chem. Chem. Phys.*, 2012, **14**, 225–233.

[16] D. Jacquemin, E. A. Perpète, G. Scalmani, M. J. Frisch, X. Assfeld, I. Ciofini and C. Adamo, *J. Chem. Phys.*, 2006, **125**, 164324.

[17] Y. Kurashige, T. Nakajima, S. Kurashige, K. Hirao and Y. Nishikitani, *J. Phys. Chem. A*, 2007, **111**, 5544–5548.

[18] B. M. Wong and J. G. Cordaro, *J. Chem. Phys.*, 2008, **129**, 214703.

[19] W. Wu, Z. Cao and Y. Zhao, *J. Chem. Phys.*, 2012, **136**, 114305.

[20] V. Barone, A. Ferretti and I. Pino, *Phys. Chem. Chem. Phys.*, 2012, **14**, 16130–16137.

[21] F. De Angelis, F. Santoro, M. K. Nazeruddin and V. Barone, *J. Phys. Chem. B*, 2008, **112**, 13181–13183.

[22] D. Jacquemin, E. Brémond, I. Ciofini and C. Adamo, *J. Phys. Chem. Lett.*, 2012, **3**, 468–471.

[23] K. Hara, Y. Tachibana, Y. Ohga, A. Shinpo, S. Suga, K. Sayama, H. Sugihara and H. Arakawa, *Sol. Energy Mater. Sol. Cells*, 2003, **77**, 89–103.

[24] Z.-S. Wang, K. Hara, Y. Dan-oh, C. Kasada, A. Shinpo, S. Suga, H. Arakawa and H. Sugihara, *J. Phys. Chem. B*, 2005, **109**, 3907–3914.

[25] D. Pant, M. Le Guennec, B. Illien and H. H. Girault, *Phys. Chem. Chem. Phys.*, 2004, **6**, 3140–3146.

[26] F. Santoro, R. Improta, A. Lami, J. Bloino and V. Barone, *J. Chem. Phys.*, 2007, **126**, 084509.

[27] F. Santoro, A. Lami, R. Improta and V. Barone, *J. Chem. Phys.*, 2007, **126**, 184102.

[28] F. Santoro, A. Lami, R. Improta, J. Bloino and V. Barone, *J. Chem. Phys.*, 2008, **128**, 224311.

[29] F. J. Avila Ferrer, J. Cerezo, J. Soto, R. Improta and F. Santoro, *Comput. Theoret. Chem.*, 2014, **1040–1041**, 328–337.

[30] V. Barone, M. Biczysko, J. Bloino, L. Carta and A. Pedone, *Comput. Theoret. Chem.*, 2014, **1037**, 35–48.

[31] F. J. Avila Ferrer, R. Improta, F. Santoro and V. Barone, *Phys. Chem. Chem. Phys.*, 2011, **13**, 17007–17012.

[32] R. A. Marcus, *J. Phys. Chem.*, 1989, **93**, 3078–3086.

[33] C. Adamo and V. Barone, *J. Chem. Phys.*, 1999, **110**, 6158–6170.

[34] M. Ernzerhof and G. E. Scuseria, *J. Chem. Phys.*, 1999, **110**, 5029–5036.

[35] T. Yanai, D. P. Tew and N. C. Handy, *Chem. Phys. Lett.*, 2004, **393**, 51–57.

[36] R. Improta, V. Barone and F. Santoro, *Angew. Chemie Int. Ed.*, 2007, **46**, 405–408.

[37] D. Jacquemin, E. Breémond, A. Planchat, I. Ciofini and C. Adamo, *J. Chem. Theory Comput.*, 2011, **7**, 1882–1892.

[38] M. D. Davari, F. J. A. Ferrer, D. Morozov, F. Santoro and G. Groenhof, *ChemPhysChem*, 2014, 1–11.

[39] F. J. Avila Ferrer, M. D. Davari, D. Morozov, G. Groenhof and F. Santoro, *ChemPhysChem*, 2014, 1–13.

[40] J. Tomasi, B. Mennucci and R. Cammi, *Chem. Rev.*, 2005, **105**, 2999–3094.

[41] R. Cammi, S. Corni, B. Mennucci and J. Tomasi, *J. Chem. Phys.*, 2005, **122**, 104513.

[42] R. Improta, in *UV-Visible Absorption and Emission Energies in Condensed Phase by PCM/TD-DFT Methods*, John Wiley & Sons, Inc., 2011, pp. 37–75.

[43] G. Scalmani, M. J. Frisch, B. Mennucci, J. Tomasi, R. Cammi and V. Barone, *J. Chem. Phys.*, 2006, **124**, 094107.

[44] M. J. Frisch, G. W. Trucks, H. B. Schlegel, G. E. Scuseria, M. A. Robb, J. R. Cheeseman, G. Scalmani, V. Barone, B. Mennucci, G. A. Petersson, H. Nakatsuji, M. Caricato, X. Li, H. P. Hratchian, A. F. Izmaylov, J. Bloino, G. Zheng, J. L. Sonnenberg, M. Hada, M. Ehara, K. Toyota, R. Fukuda, J. Hasegawa, M. Ishida, T. Nakajima, Y. Honda, O. Kitao, H. Nakai, T. Vreven, J. A. Montgomery, Jr., J. E. Peralta, F. Ogliaro, M. Bearpark, J. J. Heyd, E. Brothers, K. N. Kudin, V. N. Staroverov, R. Kobayashi, J. Normand, K. Raghavachari, A. Rendell, J. C. Burant, S. S. Iyengar, J. Tomasi, M. Cossi, N. Rega, J. M. Millam, M. Klene, J. E. Knox, J. B. Cross, V. Bakken, C. Adamo, J. Jaramillo, R. Gomperts, R. E. Stratmann, O. Yazyev, A. J. Austin, R. Cammi, C. Pomelli, J. W. Ochterski, R. L. Martin, K. Morokuma, V. G. Zakrzewski, G. A. Voth, P. Salvador, J. J. Dannenberg, S. Dapprich, A. D. Daniels, O. Farkas, J. B. Foresman, J. V. Ortiz, J. Cioslowski and D. J. Fox, *Gaussian 09 Revision A.2*, 2009, Gaussian Inc. Wallingford CT.

[45] T. Le Bahers, C. Adamo and I. Ciofini, *J. Chem. Theory Comput.*, 2011, **7**, 2498–2506.

[46] (*a*) D. Jacquemin, T. L. Bahers, C. Adamo and I. Ciofini, *Phys. Chem. Chem. Phys.*, 2012, **14**, 5383–5388; (*b*) D. Jacquemin, *Program to compute CT parameters from cube files generated by Gaussian*, 2012, downloaded from `http://www.sciences.univ-nantes.fr/CEISAM/erc/marches/?p=973` on July 2014.

[47] F. J. Avila Ferrer and F. Santoro, *Phys. Chem. Chem. Phys.*, 2012, **14**, 13549–13563.

[48] F. Duschinsky, *Acta Physicochim.: URSS*, 1937, **7**, 551–566.

[49] J. Cerezo, J. Zúñiga, A. Requena, F. J. Ávila Ferrer and F. Santoro, *J. Chem. Theory Comput.*, 2013, **9**, 4947–4958.

[50] F. Santoro, R. Improta, A. Lami, J. Bloino and V. Barone, *J. Chem. Phys.*, 2007, **126**, 169903.

[51] F. Santoro and V. Barone, *Int. J. Quantum Chem.*, 2010, **110**, 476–486.

[52] J. Tang, M. T. Lee and S. H. Lin, *J. Chem. Phys.*, 2003, **119**, 7188–7196.

[53] R. Ianconescu and E. Pollak, *J. Phys. Chem. A*, 2004, **108**, 7778–7784.

[54] J. Tatchen and E. Pollak, *J. Chem. Phys.*, 2008, **128**, 164303.

[55] Q. Peng, Y. Niu, C. Deng and Z. Shuai, *Chem. Phys.*, 2010, **370**, 215–222.

[56] J. Huh and R. Berger, *J. Phys.: Conf. Ser.*, 2012, **380**, 012019.

[57] R. Borrelli, A. Capobianco and A. Peluso, *J. Phys. Chem. A*, 2012, **116**, 9934–9940.

[58] (*a*) F. Santoro, *FCclasses, a Fortran 77 code, development version. The standard version of the code can be downloaded at http://www.pi.iccom.cnr.it/fcclasses, last accessed March 5 2015. To use the development version, necessary to run TD calculations (see ref 57b), please contact the author*, 2013; (*b*) J. Cerezo and F. Santoro, *TDspectrum, a routine for TD calculations within FCclasses*, 2013.

[59] V. Barone, J. Bloino, M. Biczysko and F. Santoro, *Journal of Chemical Theory and Computation*, 2009, **5**, 540–554.

[60] J. Bloino, M. Biczysko, F. Santoro and V. Barone, *Journal of Chemical Theory and Computation*, 2010, **6**, 1256–1274.

[61] (*a*) S. Corni, R. Cammi, B. Mennucci and J. Tomasi, *J. Chem. Phys.*, 2005, **123**, 134512; (*b*) M. Caricato, B. Mennucci, J. Tomasi, F. Ingrosso, R. Cammi, S. Corni and G. Scalmani, *J. Chem. Phys.*, 2006, **124**, 124520.

[62] R. Improta, G. Scalmani, M. J. Frisch and V. Barone, *J. Chem. Phys.*, 2007, **127**, 074504.

[63] N. M. Correa and N. E. Levinger, *J. Phys. Chem. B*, 2006, **110**, 13050–61.

[64] V. Amendola, L. Fabbrizzi, C. Mangano, H. Miller, P. Pallavicini, A. Perotti and A. Taglietti, *Angew. Chemie Int. Ed.*, 2002, **41**, 2553–2556.

[65] X. Liu, J. M. Cole and K. S. Low, *J. Phys. Chem. C*, 2013, **117**, 14723–14730.

[66] A. Charaf-Eddin, A. Planchat, B. Mennucci, C. Adamo and D. Jacquemin, *J. Chem. Theory Comput.*, 2013, **9**, 2749–2760.

[67] A. Dreuw and M. Head-Gordon, *Chem. Rev.*, 2005, **105**, 4009–4037.

[68] D. W. Silverstein and L. Jensen, *J. Chem. Phys.*, 2012, **136**, 064111.

[69] A. Petrone, J. Cerezo, F. J. Avila Ferrer, R. Improta, N. Rega and F. Santoro, *J. Phys. Chem. A*, submitted.

[70] H. Shirota and K. Horie, *J. Phys. Chem. B*, 1999, **103**, 1437–1443.

[71] F. J. Avila Ferrer, J. Cerezo, E. Stendardo, R. Improta and F. Santoro, *J. Chem. Theory Comput.*, 2013, **9**, 2072–2082.

Table 1 – Vertical excitation energies (E^{VT}, eV) computed at CAM-B3LYP/6-31G(d) and PBE0/6-31G(d) levels in EtOH according to the linear-response (LR) and state-specific (SS) implementation of PCM in non-equilibrium (*neq*) regime.[a].

Dye	E^{TV}(LR)		E^{VT}(SS)	
	CAM	PBE0	CAM	PBE0
c343(I)	3.447	3.252	3.345	3.164
nkx-2311	2.815	2.543	2.746	2.504
nkx-2398	3.299	3.050	3.241	3.000
nkx-2586	2.683	2.313	2.560	2.228
nkx-2753	2.757	2.322	2.594	2.163

Notes: a) Energies computed as the difference between $S_0(eq)$ and $S_1(neq)$.

Table 2 – CT parameters derived from the GS and ES charge densities computed with CAM-B3LYP/6-31G(d) at the minimum of the GS (GSmin) and the ES (ESmin) surfaces with LR-PCM: amount electron charge transfer (Q_{CT}, in electron charge units, *e*), distance between barycenter (D_{CT}, in Å) and spread index along *x* axis (H_x, in Å), which is, approximately, the axis connecting the two barycenters. The difference between the electric dipole moments in the initial and final states is also reported ($|\Delta\mu|$, in Debye).

	GSmin				ESmin			
Dye	Q_{CT}	D_{CT}	H_x	$\lvert\Delta\mu\rvert$	Q_{CT}	D_{CT}	H_x	$\lvert\Delta\mu\rvert$
CAM-B3LYP								
c343	0.51	2.31	2.42	5.6	0.47	2.05	2.38	4.6
nkx-2311	0.60	3.45	3.80	10.0	0.51	2.51	3.63	6.2
nkx-2398	0.54	2.74	3.05	7.1	0.48	2.12	2.98	4.8
nkx-2586	0.64	4.37	4.56	13.4	0.52	3.12	4.31	7.8
nkx-2753	0.67	4.28	4.57	13.7	0.55	3.20	4.31	8.4
PBE0								
c343	0.44	2.36	2.44	5.0	0.47	2.53	2.44	5.8
nkx-2311	0.49	3.60	3.82	8.5	0.48	3.68	3.81	8.5
nkx-2398	0.47	2.96	3.17	6.6	0.45	2.85	3.14	6.1
nkx-2586	0.54	4.66	4.51	12.1	0.51	4.49	4.47	11.0
nkx-2753	0.62	4.80	5.53	14.3	0.55	4.45	4.48	11.8

Table 3 – Computed standard deviation $\sigma(\mathrm{cm}^{-1})^a$ for the different contributions to the absorption spectra lineshapes in EtOH at 300 K evaluated at TD-CAM-B3LYP/6-31G(d) level.

Dye	$\sigma_{vib}{}^a$	σ_m(PCM)	σ_{tot}
c343	1009 (959)	549	1149
nkx-2311	1345 (1285)	698	1516
nkx-2398	1256 (1150)	608	1396
nkx-2586	1714 (1642)	917	1944
nkx-2753	2000 (1814)	1041	2255

Notes: a) Vibrational broadening at 0 K is included in parentheses.

Table 4 – Maxima (eV) of the experimental spectra and of the spectra computed at CAM-B3LYP/6-31G(d) and PBE0/6-31G(d) level of theory in EtOH

Dye	ω_{exp}^{max}	ω_{com}^{max}(CAM)	ω_{com}^{max}(PBE0)
c343	2.777	3.196	2.998
nkx-2311	2.475	2.617	2.395
nkx-2398	2.753	3.078	2.852
nkx-2586	2.435	2.466	2.148
nkx-2753	2.487	2.578	2.098

Table 5 – Full widths at half maximum (in cm^{-1}) of the total computed absorption lineshapes (W_{tot}) and of the solvent contributions (W_m) obtained at CAM-B3LYP/6-31G(d) level in EtOH.

Dye	Exp	W_m		W_{tot}	
		CAM	PBE0	CAM	PBE0
c343	3130	1293	1141	2070	2150
nkx-2311	4082	1643	1242	3036	1688
nkx-2398	2962	1433	1259	2809	1808
nkx-2586	4342	2160	1461	4244	1995
nkx-2753	4483	2453	1723	5052	2848

The reported experimental FWHMs are obtained from the spectra in refs. 9, 10, 23 and 24, after converting them into lineshape (see Figure 4).

Table 6 – Computed values of the FWHM (in cm^{-1}) of the medium (W_m) and of the total spectra W_{tot} for coumarin c343 in different solvents.

Solvent	Exp.	W_m		W_{tot}	
		CAM	PBE0	CAM	PBE0
EtOH	3130	1293	1141	2070	2150
DCE	2105	1153	1023	1885	1760
ACN	2358	1324	1172	2020	1915

The reported experimental FWHMs are obtained from the spectra in refs. 25 (DCE), 9 (EtOH) and 70 (ACN), after converting them into lineshape (see Figure 6).

Table 7 – Solvent reorganization energies (λ, cm^{-1}) computed at CAM-B3LYP/6-31G(d) and PBE0/6-31G(d) levels in EtOH according to the state-specific (SS) implementation of PCM in non-equilibrium (*neq*) regime. Reorganization energies in the excited states are evaluated at the Frank-Condon (FC) point (i.e. at the GS equilibrium structure, GSmin) and at the ES optimized structure (ESmin). For c343, the solvent reorganization energies in DCE and ACN are also included.

Dye	λ_{SS}^{sol}(FC)		λ_{SS}^{sol}(ESmin)	
	CAM	PBE0	CAM	PBE0
EtOH				
c343	728	567	509	732
nkx-2311	1175	671	355	565
nkx-2398	894	690	387	532
nkx-2586	2030	929	384	640
nkx-2753	2618	1293	484	778
DCE				
c343	579	455	391	571
ACN				
c343	764	597	532	766

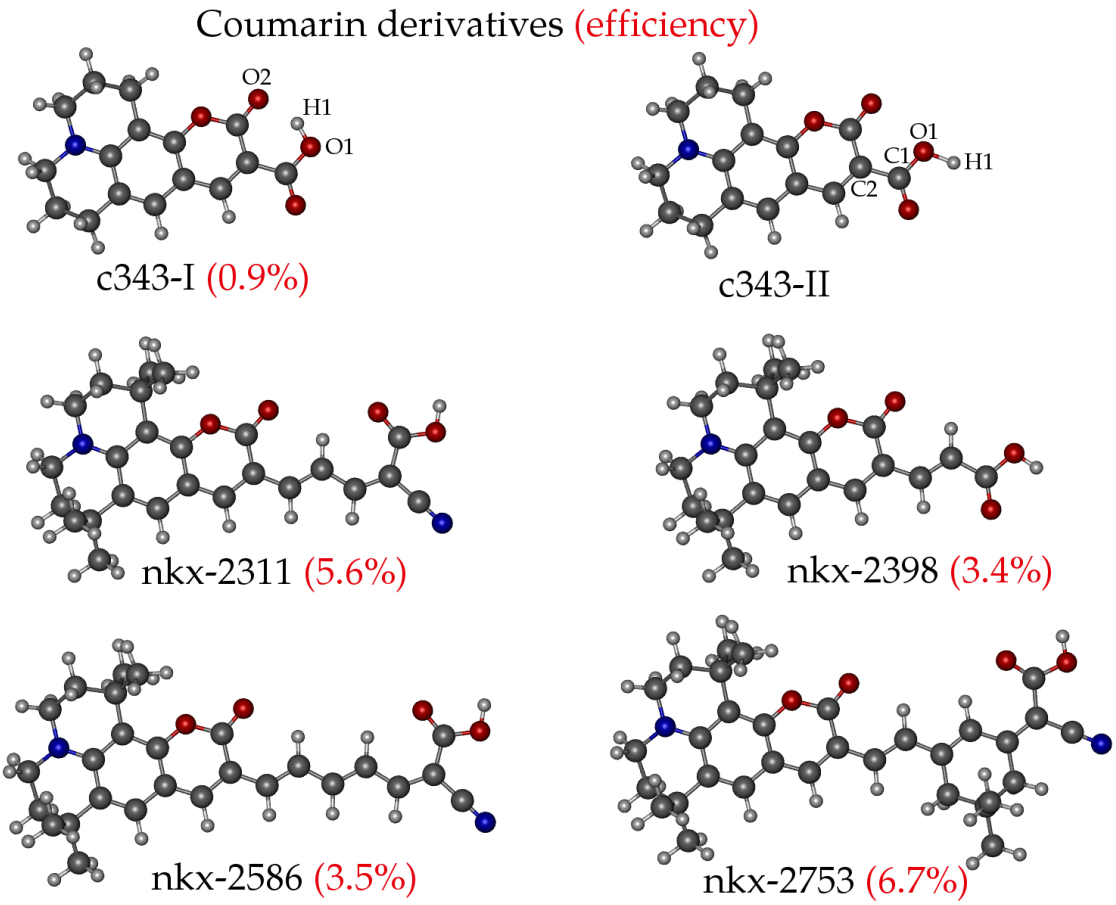

Figure 1 – Coumarin derivatives investigated in this work. In red, DSSC efficiency taken from ref. 23 for c343, nkx-2398, nkx-2311 and nkx-2586, and from ref. 24 for nkx-2753.

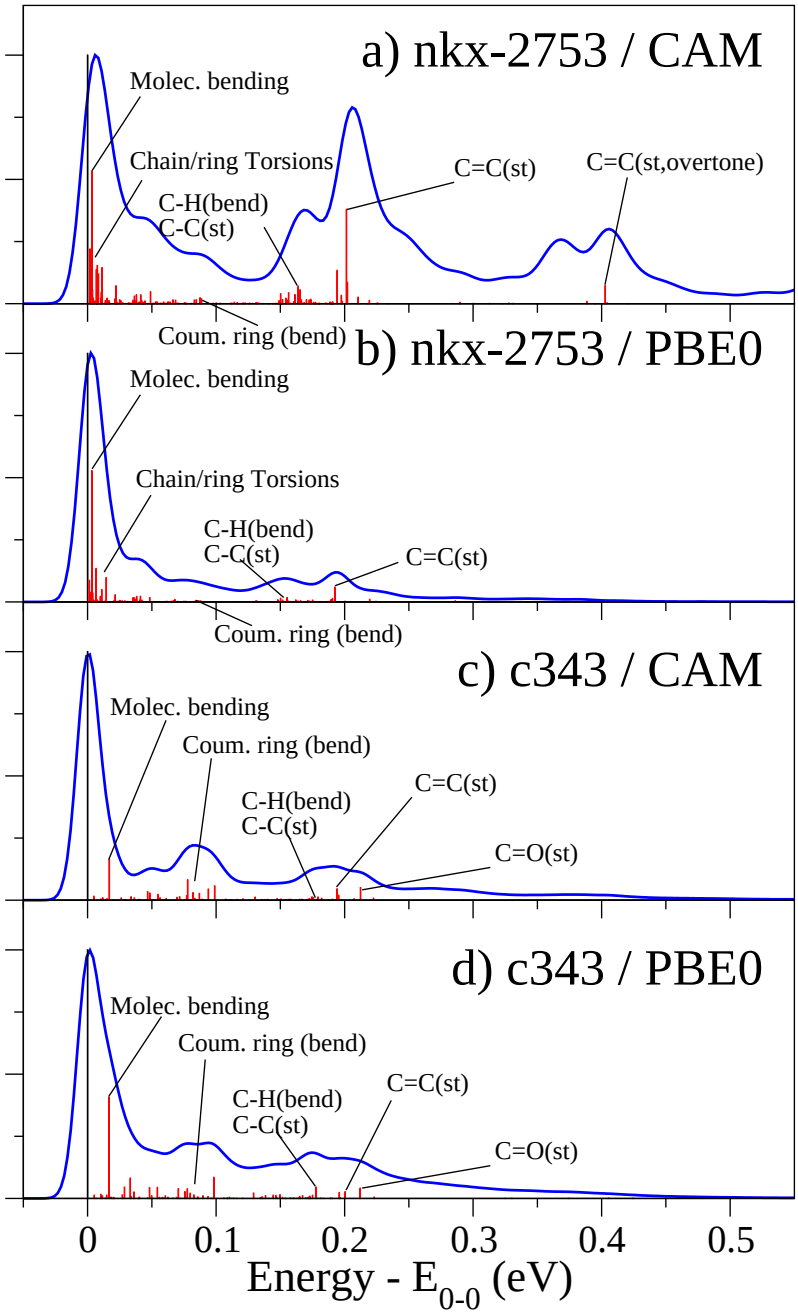

Figure 2 – TI spectra computed at TD CAM-B3LYP/6-31G(d) and TD PBE0/6-31G(d) for c343 and nkx-2753 in ethanol at 0 K, including the most intense Class C_1 transitions (only one mode excited in S_1)[26] and a brief description of the the most relevant modes involved. Molec. bending.: in-plane bending of the whole molecule along the longest molecular axis; Chain/ring torsions: collective movements involving the torsion of C-C bonds within the ring or/and the lateral chain; Cou. ring (bend): coupled bending movements involving the atoms within the coumarin ring; C=C(st), C-C(st): stretching of C=C and C-C bonds of the conjugated chain; C=O(st): stretching of the C=O bond on coumarin ring. Animations of these modes are included in the ESI. The lineshape spectra (blue) are convoluted with a Gaussian function with FWHM of 0.02 eV.

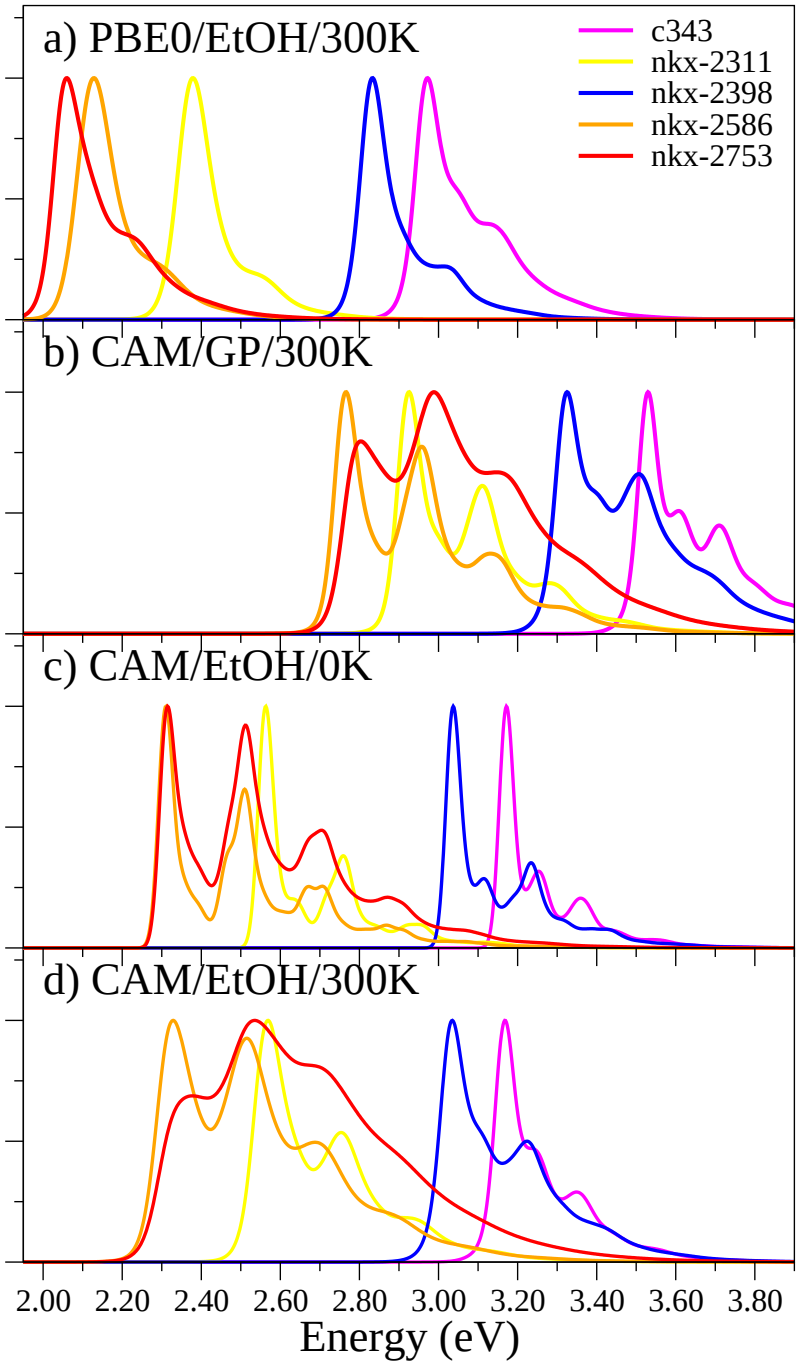

Figure 3 – Computed vibrationally resolved absorption spectra for the 5 coumarins under study with different computational/environmental settings: using PBE0 and PCM (EtOH) at 300 K (a); using CAM-B3LYP functional gas phase at 300 K (b); and using the same functional with PCM (EtOH) at 0 K (c) and 300 K (d). All spectra are convoluted with a Gaussian of FWHM=0.04 eV.

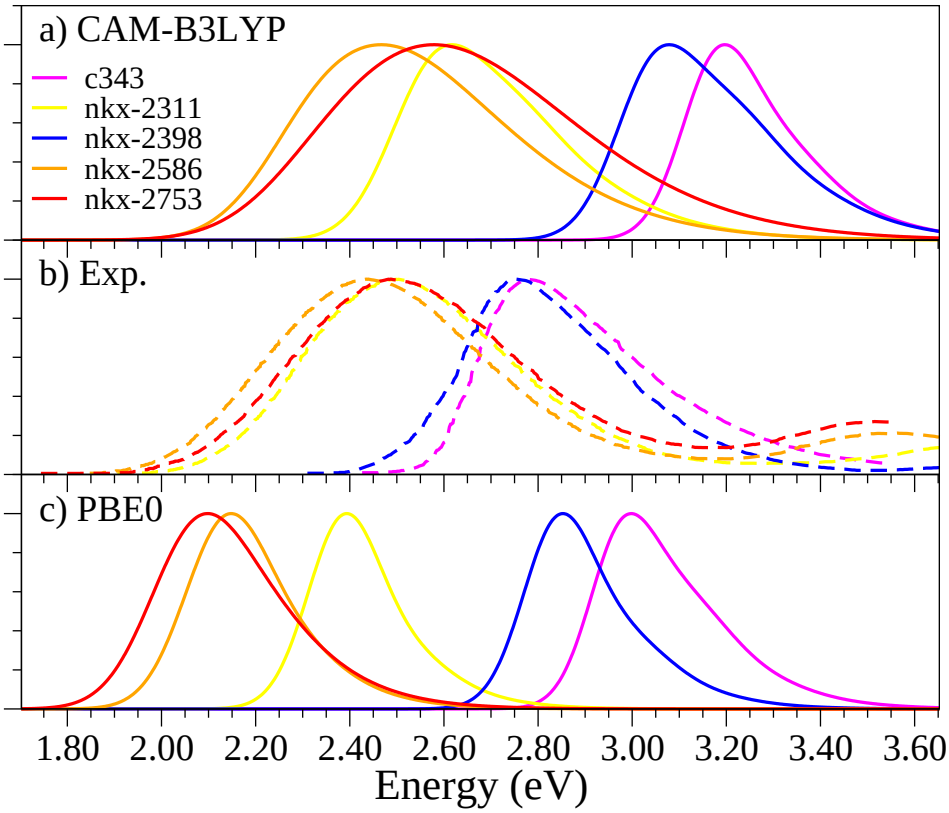

Figure 4 – Normalized absorption lineshapes for the coumarins c343, nkx-2311, nkx-2398, nkx-2586 and nkx-2753 in EtOH at 300 K. Vibronic spectra convoluted with a Gaussian whose FWHM corresponds to the inhomogeneous broadening computed at SS-PCM level. a) CAM-B3LYP/6-31G(d) and c) PBE0/6-31G(d) results. In central panel b), the experimental lineshapes from refs. 9, 10, 23 and 24 are also included.

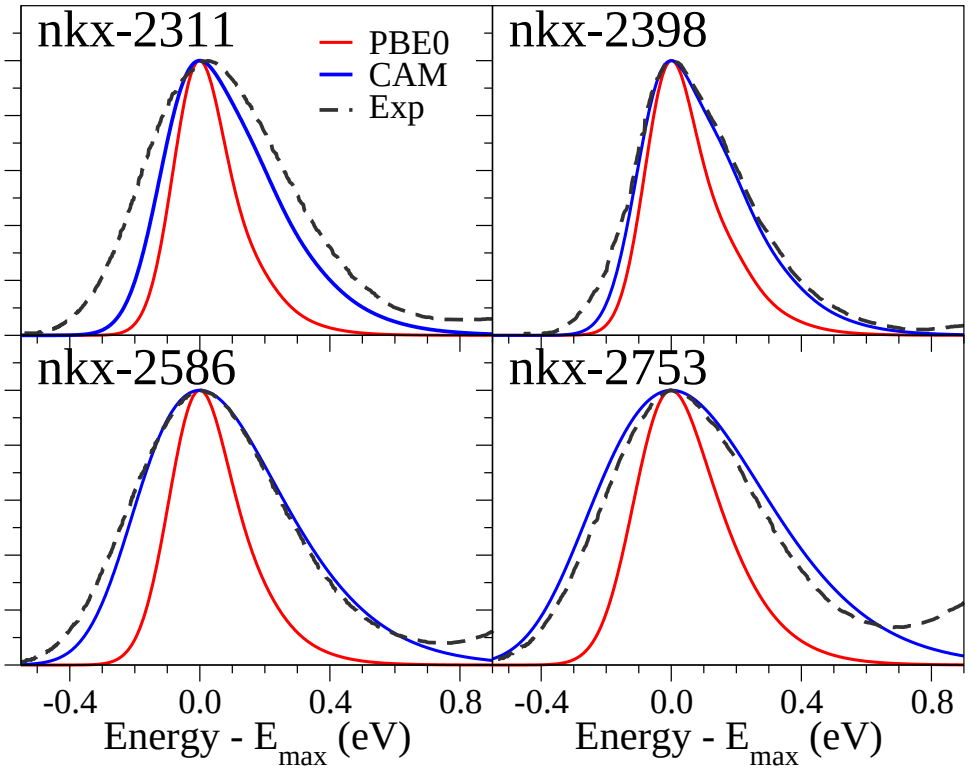

Figure 5 – Computed absorption spectra of all coumarins studied in this paper, except c343, simulated at 300 K with CAM-B3LYP and PBE0 vibronic structure and broadenings, along with the experimental ones. All bands are shifted by the spectra maxima in order to facilitate the comparison of the shapes.

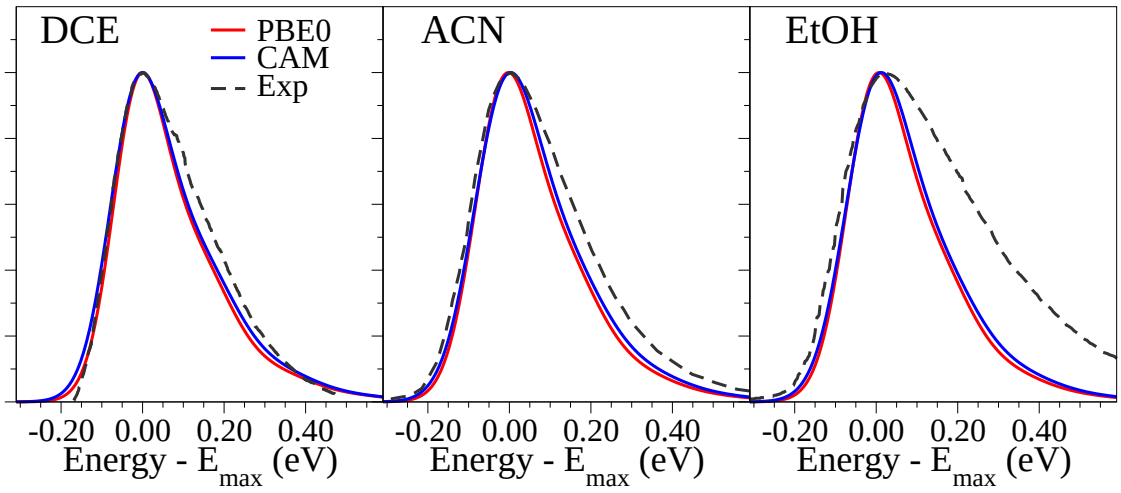

Figure 6 – Computed absorption spectrum of c343 in DCE (left), ACN (center) and EtOH (right), at 300 K with CAM-B3LYP and PBE0 vibronic structure and broadenings, along with the experimental spectra from refs. 25 (DCE), 9 (EtOH) and 70 (ACN). All bands are shifted by the spectra maxima in order to facilitate the comparison of the shapes.

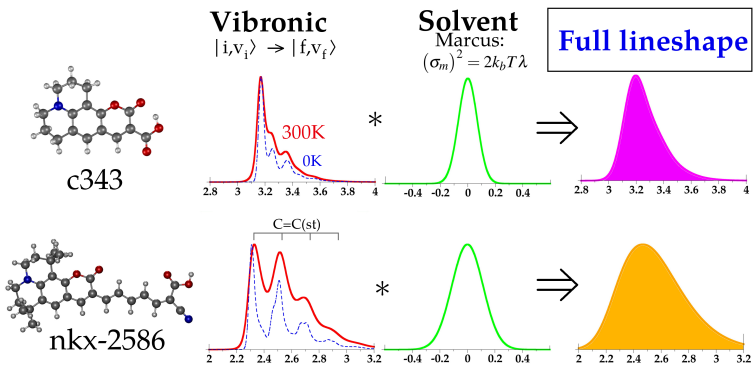

Figure TOC – Individuation of vibronic and solvent contributions to the spectra of a family of coumarin dyes helps to understand the main differences in their lineshapes.

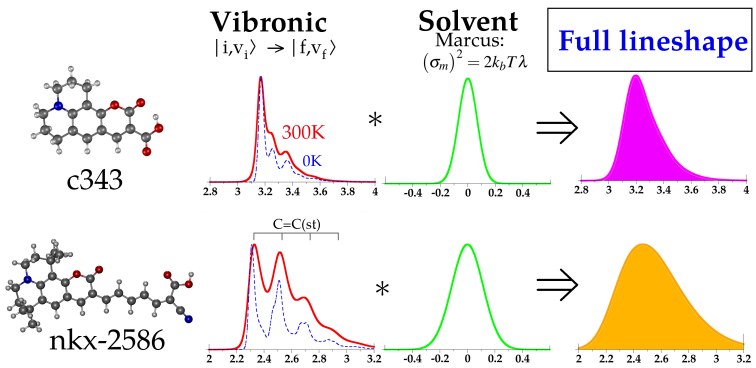

Figure TOC – Individuation of vibronic and solvent contributions to the spectra of a family of coumarin dyes helps to understand the main differences in their lineshapes.